Routes to energy dissipation for geostrophic flows in the Southern Ocean

Maxim Nikurashin[*][†]**, Geoffrey K. Vallis and Alistair Adcroft**

The ocean circulation is forced at a global scale by winds and fluxes of heat and fresh water. Kinetic energy is dissipated at much smaller scales in the turbulent boundary layers and in the ocean interior[1,2], where turbulent mixing controls the transport and storage of tracers such as heat and carbon dioxide[3,4]. The primary site of wind power input is the Southern Ocean, where the westerly winds are aligned with the Antarctic Circumpolar Current[5]. The potential energy created here is converted into a vigorous geostrophic eddy field through baroclinic instabilities. The eddy energy can power mixing in the ocean interior[6–8], but the mechanisms governing energy transfer to the dissipation scale are poorly constrained. Here we present simulations that simultaneously resolve meso- and submeso-scale motions as well as internal waves generated by topography in the Southern Ocean. In our simulations, more than 80% of the wind power input is converted from geostrophic eddies to smaller-scale motions in the abyssal ocean. The conversion is catalysed by rough, small-scale topography. The bulk of the energy is dissipated within the bottom 100 m of the ocean, but about 20% is radiated and dissipated away from topography in the ocean interior, where it can sustain turbulent mixing. We conclude that in the absence of rough topography, the turbulent mixing in the ocean interior would be diminished.

Geostrophic eddies, constituting a large part of the kinetic energy of the ocean, are strongly constrained by Earth's rotation and tend to transfer energy towards larger scales[9,10], whereas dissipation of kinetic energy in the ocean occurs at small, $O(1)$ cm, scales. Various mechanisms have been suggested for how energy is extracted from geostrophic eddies and transferred to unbalanced motions from where it may be cascaded to smaller dissipation scales. For example, western boundaries in ocean basins, where eddies can scatter into Kelvin wave hydraulics[11], have been shown to be sites of elevated eddy-energy loss[12]. In the Southern Ocean, where lateral boundaries are absent, geostrophic eddies must dissipate either in the ocean interior or through interaction with the bottom boundary[13,14]. Flow over rough small-scale topography can excite internal gravity waves that radiate energy away from topography into the ocean interior[15,16]. Away from the boundaries, surface processes such as frontogenesis, frontal and mixed layer instabilities, which transfer energy to smaller submesoscale motions, have all been suggested as possible routes for eddy-energy dissipation[17,18]. Although all of these processes extract energy from geostrophic flows, it remains unclear whether one process dominates eddy-energy dissipation and contributes to turbulence and mixing in the ocean interior.

Away from the surface and bottom boundary layers, enhanced turbulence and mixing in the ocean have been observed in the abyssal ocean in regions with rough small-scale topography[7,19–21].
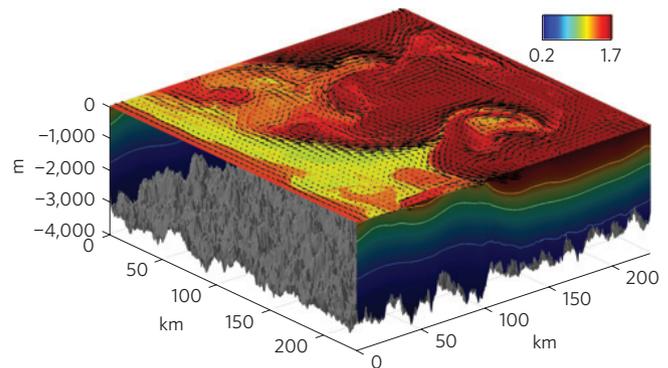

Figure 1 | A snapshot of temperature in (°C), surface currents and bottom topography after 40 days of simulations. The interior temperature isolines of 0.5, 0.9 and 1.3 °C are shown in light blue, green and orange colours, respectively.

These observations suggest that enhanced turbulence may be sustained by breaking of internal waves radiating from rough small-scale topography. Generation of internal waves at rough topography results in the direct energy conversion from large-scale, geostrophically balanced flows into unbalanced internal waves that can subsequently transfer their energy to small dissipation scales through nonlinear interactions and wave breaking. Our goal in this study is to understand the energetic pathways for such flows. Specifically, we seek to understand how various motions in regions away from lateral boundaries and tall topographic features can extract energy from geostrophic flows and radiate this energy into the ocean interior. To this end, we present results from two numerical experiments, one with realistically rough topography and the other with a flat lower boundary. The experiments simulate the dynamics of the wind-driven geostrophic flow, analogous to a front of the Antarctic Circumpolar Current, and explicitly resolve the dynamics of meso-, submeso- and topographic internal wave scale motions. Details of the experimental set up are given in the Methods.

A snapshot from the rough-topography simulation, showing surface temperature and currents, meridional cross-section of temperature, and bottom topography is shown in Fig. 1. The snapshot illustrates a meandering front with warm fluid in the north and cold in the south (and the experiment with a flat bottom is very similar in this regard). Deep isopycnals in the frontal region are steeply sloped, as a result of geostrophic, thermal wind balance. The snapshot captures a detached, cold-core, cyclonic eddy with the horizontal scale of 30–50 km (the Rossby radius of
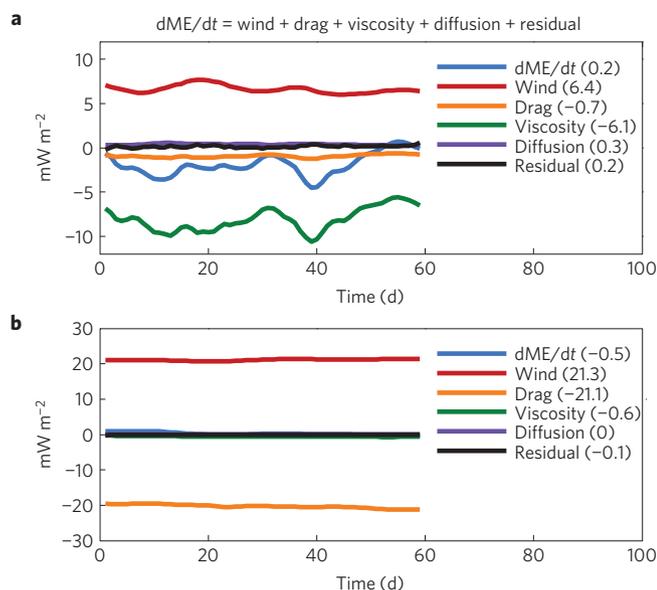
AOS Program, Princeton University, Princeton, New Jersey 08540, USA. [†]Present address: Institute for Marine and Antarctic Studies, University of Tasmania, Hobart, Tasmania 7001, Australia. *e-mail: man@alum.mit.edu.

Figure 2 | Mechanical, a sum of kinetic and potential, energy budget terms in (mW m^{-2}) as a function of time. a,b, Energy budgets from rough-topography (**a**) and flat-bottom (**b**) simulations: evolution of mechanical energy (blue), wind power input (red), dissipation by the bottom drag (orange), dissipation by viscous friction (green) and changes in potential energy due to diffusion (purple). Values averaged over the last 10 days of simulations are shown in parenthesis.

deformation in the experiment is about 20 km) as well as several smaller, submesoscale, warm- and cold-core eddies. The bottom topography is multichromatic, randomly generated with the same spectral characteristics as topography observed in the Drake Passage region of the Southern Ocean[16] and includes horizontal scales from 50 km down to 1 km.

The energetics of the flow in the two simulations are presented in Fig. 2 showing the evolution of the volume-integrated mechanical (that is, a sum of kinetic and potential) energy budget terms. The energy budgets are closed to within a few per cent of the wind power input terms. Both simulations are well equilibrated. In the rough-topography simulation, there is a leading-order balance between the wind power input at the surface of 6.4 mW m^{-2} and interior viscous dissipation of 6.1 mW m^{-2}. Dissipation due to bottom drag, which parameterizes unresolved turbulence in the bottom boundary layer, is small, 0.7 mW m^{-2}, compared with the viscous dissipation by resolved motions. The effect of diffusion, computed as a change in the unavailable potential energy[22,23] (that is, potential energy of a motionless fluid) and thus including the effects of both explicit and spurious numerical diffusion, is negligible, 0.3 mW m^{-2}. The energetics of the rough-topography simulation suggest that the wind power input, generated by the wind stress acting on the time-mean flow at the surface, is primarily dissipated by interior viscous friction acting on resolved motions. Viscous friction, which parameterizes subgrid-scale processes, is scale dependent: it acts primary on small-scale motions with large velocity gradients. In the simulations, the Reynolds number of geostrophic eddies, estimated at the deformation scale of 20 km, is $O(10^4)$, implying that geostrophic eddies are inertial and essentially inviscid. Hence, to equilibrate, geostrophic eddies must transfer their energy to smaller-scale motions that can then be dissipated by viscous friction. In the flat-bottom simulation, on the other hand, viscous dissipation is small, implying that there is no effective mechanism for the generation of small-scale motions and therefore the bulk of the wind power input is dissipated by the bottom drag. That is, the spontaneous generation of unbalanced
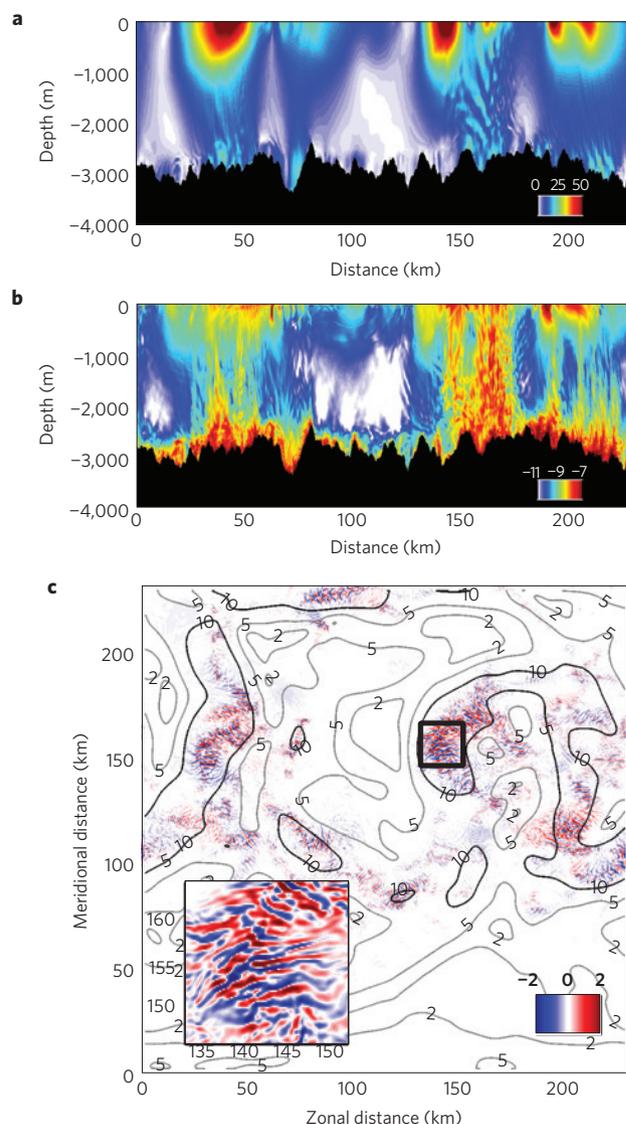

Figure 3 | Snapshots after 40 days in the rough-bottom simulation. a,b, Zonal sections of speed (cm s^{-1}; **a**) and energy dissipation dissipation (log$_{10}$(W kg^{-1}); **b**) at $y = 170$ km. **c**, Horizontal section at 2 km depth of vertical velocity (cm s^{-1}; blue/red) and 5 km low-pass-filtered horizontal flow speed (cm s^{-1}; contours). The inset plot is a zoom-in on the region shown with the thick black line.

motion from geostrophic flows in the ocean interior is far less efficient than the generation of unbalanced flow through eddy–topographic interactions.

The equilibration of the flow changes markedly between the two simulations: in the flat-bottomed simulation, the wind stress is completely balanced by the bottom drag rather than the topographic form stress as in the rough-topography simulation, and the wind power input is nearly balanced by the bottom drag work against the bottom flow rather that the interior viscous dissipation. As a result, the system equilibrates with higher magnitude of the flow and therefore higher wind power input.

Vertical and horizontal representations of the flows in the rough-topography simulation are illustrated in Fig. 3. The top two panels show zonal cross-sections of kinetic energy and viscous energy dissipation, emphasizing large- and small-scale motions, respectively. The kinetic energy of the flow is dominated by frontal meanders and mesoscale eddies. Consistent with observations[24,25], the surface speed of geostrophic eddies exceeds 50 cm s^{-1}, whereas
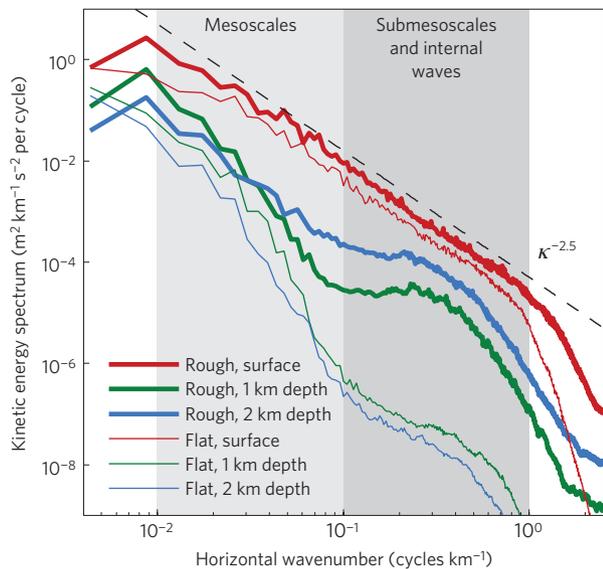
Figure 4 | Horizontal wavenumber kinetic energy spectra. Spectra computed at the surface (red), 1 km depth (green) and 2 km depth (blue) from rough- (thick lines) and flat- (thin lines) topography simulations. Characteristic wavenumber ranges corresponding to mesoscale eddies (light-grey shading) and submesoscale and internal wave motions (dark-grey shading) are shown. The spectrum slope of −2.5 is shown by the dashed black line.

Figure 5 | Zonal sections of time-averaged energy dissipation in dissipation in $\log_{10}(W\,kg^{-1})$. a,b, Energy dissipation from rough- (**a**) and flat- (**b**) topography simulations.

the temporal and zonal mean flow speed (not shown) is only about $10\,cm\,s^{-1}$. Although eddying geostrophic flows are surface intensified, they are characterized by relatively strong bottom speeds of $5–10\,cm\,s^{-1}$. In addition, there are smaller-scale motions in both the upper and deep ocean. In the upper ocean, the smaller-scale motions are primarily submesoscale fronts and eddies that are limited to the upper few hundred meters. In the deep ocean, there are radiating and trapped topographic internal gravity waves and hydraulic flows at low levels behind steep topographic features. The energy dissipation distribution is dominated by the small-scale motions. The dissipation is enhanced in the deep ocean above topography, in the ocean interior in places of enhanced wave activity, and in the upper ocean in regions of small submesoscale fronts and eddies. Again consistent with observational estimates for the Southern Ocean[7], the energy dissipation in the deep ocean reaches values up to $10^{-8}\,W\,kg^{-1}$ (background level of energy dissipation for the typical Southern Ocean stratification of $10^{-3}\,s^{-1}$ is $10^{-10}\,W\,kg^{-1}$). Generally, the results show that there is a tendency for internal waves and energy dissipation to be enhanced in regions of strong bottom large-scale flows, suggesting that small-scale motions in the deep ocean are generated by abyssal geostrophic flows interacting with rough small-scale topography. This is illustrated more quantitatively in Fig. 3c showing a horizontal section of the vertical velocity and low-pass-filtered horizontal speed at 2 km depth. We see patches of internal waves with horizontal scales of a few kilometres and amplitudes of $1–3\,cm\,s^{-1}$ co-located with strong ($5–10\,cm\,s^{-1}$), deep geostrophic flow.

To illustrate the role of rough topography in generation of small-scale unbalanced motion, Fig. 4 shows horizontal wavenumber spectra from both simulations. The surface spectra from both rough- and flat-topography simulations show an inertial range of scales from roughly the 100 km scale, where energy is injected into the system by wind, down to the model viscous range at scales smaller than 0.5–1 km, where energy is removed by friction. The slope of the surface spectra is −2.5, which is roughly consistent with previous numerical studies[18,26]. In the deep ocean, the kinetic energy is generally lower than at the surface. With rough topography
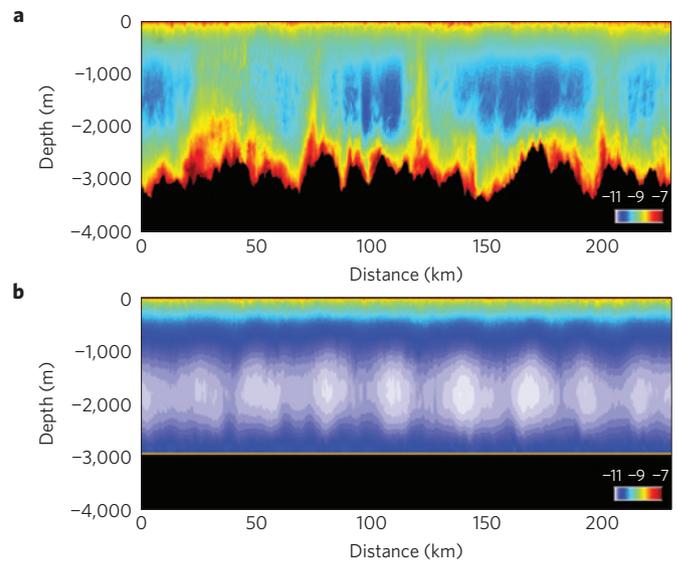
there is a broad energy enhancement in the deep ocean at a 2–4 km scale, corresponding to radiating internal gravity waves generated at topography. This enhancement is absent in the flat-bottom simulation, with energy levels at those scales being some two orders of magnitude lower than in the rough-topography experiment.

Evidently, although internal waves can be potentially generated spontaneously by geostrophic turbulence in the upper ocean, their generation is in fact dominated by flows over rough small-scale topography in the deep ocean. Finally, to further contrast rough-topography and flat-bottom simulations, Fig. 5 shows a zonal section of the distribution of time-averaged viscous energy dissipation throughout the domain from both experiments. In the rough-topography simulation, the viscous energy dissipation is dominated by the deep ocean: $5\,mW\,m^{-2}$, or 80% of the total volume-integrated energy dissipation, takes place below 1 km depth. About $1\,mW\,m^{-2}$, or 20% of the total energy dissipation, takes place below 1 km depth and 100 m or more away from the bottom, implying that it is radiated into the ocean interior presumably in the form of internal gravity waves. In contrast, in the flat-bottomed simulation, the bulk of the wind power input is dissipated by the bottom drag with only a few per cent dissipating in the ocean interior.

The wind power input into the ocean circulation (dominated by the Southern Ocean) raises the potential energy of the flow, which is converted into a vigorous geostrophic eddy field. Geostrophic eddies are mesoscale features of the ocean circulation and are neither dissipated directly by friction nor can their energy be directly cascaded to smaller dissipation scales. Rather, to equilibrate, geostrophic eddies must transfer their energy to smaller-scale unbalanced motion either through generation of submesoscale motions in the upper ocean or by interaction with the bottom boundary. Using high-resolution simulations with parameters typical for the Southern Ocean, we show that the interaction of geostrophic eddies with rough small-scale topography is the dominant energy pathway to smaller, unbalanced motions in the Southern Ocean, accounting for the dissipation of up to 80% of the wind power input. The rest of the energy dissipates in the upper few hundred meters of the ocean and is attributed to the generation of fronts and submesoscale eddies. The wind power input, transferred from geostrophic eddies to unbalanced internal gravity waves and radiated into the stratified ocean interior, can ultimately sustain

interior diapycnal mixing, drive meridional overturning circulation and hence affect ocean circulation and climate.

Methods

Model configuration. We employ the non-hydrostatic configuration of the Massachusetts Institute of Technology general circulation model[27] (MITgcm). The domain used in the simulations is three-dimensional, zonally periodic with a uniform horizontal and vertical resolution of 200 and 20 m, respectively. The horizontal size of the domain is 230 km in both zonal and meridional direction and the total depth is 4 km. Solid walls with the free-slip, no-flux boundary conditions are imposed at the northern and southern boundaries. The stratification used in the simulations has an idealized shape chosen to match observations in the Southern Ocean[7]: the stratification is $N = 7 \times 10^{-4} \text{ s}^{-1}$ in the bottom-most 1–2 km, increasing by a factor of 3 in the upper kilometre. A Coriolis frequency of $f = 1.5 \times 10^{-4} \text{ s}^{-1}$ is used. The Laplacian horizontal and vertical viscosity values of $A_h = 1 \text{ m}^2 \text{ s}^{-1}$ and $A_v = 10^{-3} \text{ m}^2 \text{ s}^{-1}$ are used. The simulation is forced by applying a zonal, cosine-shaped wind stress with a maximum of 0.15 N m^{-2} in the middle of the domain and zero values at the northern and southern boundaries. A free-slip bottom boundary condition with quadratic drag, $C_d = 2 \times 10^{-3}$, is used. Both horizontal and vertical diffusivities are set to $10^{-5} \text{ m}^2 \text{ s}^{-1}$. Note that these values of diffusivity and viscosity correspond to large turbulent Prandtl numbers (the ratio of viscosity to diffusivity) implying that energy at small scales is dissipated primarily by viscous (frictional) processes with the efficiency of mixing processes being small. All experiments are initiated from an equilibrated lower, 480 m, horizontal resolution simulation and run for two months to a statistically steady state.

Bottom topography. The topography used in the rough-topography simulation is synthetically generated with the same spectral characteristics as topography observed in the Drake Passage region of the Southern Ocean[16]. Synthetic topography is computed as a sum of Fourier modes with amplitudes given by the two-dimensional topographic spectrum and random phases. The topography includes horizontal scales in the range from 1 to 50 km, which, according to linear theory, accounts for most of the topographic internal wave energy radiation[16]. In the flat-bottom simulation, total depth is equal to the mean depth of 3,000 m from the rough-topography simulation.

Energy budget. Forming kinetic and potential energy equations from the primitive equations solved by the model, adding them and integrating over the volume, we obtain

$$\frac{\partial}{\partial t}\langle \text{ME} \rangle = \frac{\partial}{\partial t}\left(\langle \text{KE} \rangle + \langle \text{PE} \rangle\right) = \overline{\boldsymbol{\tau}_w \cdot \mathbf{u}|_{\text{top}}} - \overline{\boldsymbol{\tau}_d \cdot \mathbf{u}|_{\text{bot}}} - \langle \varepsilon \rangle$$

where the terms on the left-hand side are the evolution of kinetic energy, $\text{KE} = (1/2)\rho \mathbf{u} \cdot \mathbf{u}$, computed using the flow velocity field $\mathbf{u} = (u, v, w)$, and potential energy, $\text{PE} = \rho g z$, computed from the density field ρ. Terms on the right-hand side are the surface power input by the wind stress $\boldsymbol{\tau}_w$, power output by the bottom drag $\boldsymbol{\tau}_d$, and dissipation of kinetic energy ε given by

$$\varepsilon = \rho A_h \left[\left(\frac{\partial \mathbf{u}}{\partial x}\right) \cdot \left(\frac{\partial \mathbf{u}}{\partial x}\right) + \left(\frac{\partial \mathbf{u}}{\partial y}\right) \cdot \left(\frac{\partial \mathbf{u}}{\partial y}\right) \right] + \rho A_v \left(\frac{\partial \mathbf{u}}{\partial z}\right) \cdot \left(\frac{\partial \mathbf{u}}{\partial z}\right)$$

The effect of both explicit and spurious diffusion on the flow energetics is small (Fig. 2) and hence neglected. The brackets and over-lines represent the total volume and surface integrals, respectively.

References

1. Wunsch, C. & Ferrari, R. Vertical mixing, energy, and the general circulation of the oceans. *Ann. Rev. Fluid Mech.* **36,** 281–314 (2004).
2. Hughes, G. O., Hogg, A. & Griffiths, R. W. Available potential energy and irreversible mixing in the meridional overturning circulation. *J. Phys. Oceanogr.* **39,** 3130–3146 (2009).
3. Sarmiento, J. L. & Toggweiler, J. R. A new model for the role of the oceans in determining atmospheric $p\text{CO}_2$. *Nature* **308,** 621–624 (1984).
4. Sarmiento, J. L., Gruber, N., Brzezinski, M. A. & Dunne, J. P. High-latitude controls of thermocline nutrients and low latitude biological productivity. *Nature* **427,** 56–60 (2004).
5. Wunsch, C. The work done by the wind on the oceanic general circulation. *J. Phys. Oceanogr.* **28,** 2331–2339 (1998).
6. Ferrari, R. & Wunsch, C. Ocean circulation kinetic energy—reservoirs, sources and sinks. *Ann. Rev. Fluid Mech.* **41,** 253–282 (2009).
7. Naveira Garabato, A., Polzin, K. L., King, B. A., Heywood, K. J. & Visbeck, M. Widespread intense turbulent mixing in the Southern Ocean. *Science* **303,** 210–213 (2004).
8. Nikurashin, M. & Ferrari, R. Global energy conversion rate from geostrophic flows into internal lee waves in the deep ocean. *Geophys. Res. Lett.* **38,** L08610 (2011).
9. Charney, J. G. Geostrophic turbulence. *J. Atmos. Sci.* **28,** 1087–1095 (1971).
10. Vallis, G. K. *Atmospheric and Oceanic Fluid Dynamics* (Cambridge Univ. Press, 2006).
11. Hogg, A., Dewar, W., Berloff, P. & Ward, M. Kelvin wave hydraulic control induced by interactions between vortices and topography. *J. Fluid Mech.* **687,** 194–208 (2011).
12. Zhai, X., Johnson, H. & Marshall, D. Significant sink of ocean-eddy energy near western boundaries. *Nature Geosci.* **3,** 608–612 (2010).
13. Sen, A., Scott, R. B. & Arbic, B. K. Global energy dissipation rate of deep-ocean low-frequency flows by quadratic bottom boundary layer drag: Computations from current-meter data. *Geophys. Res. Lett.* **35,** L09606 (2008).
14. Arbic, B. K. *et al.* Estimates of bottom flows and bottom boundary layer dissipation of the oceanic general circulation from global high-resolution models. *J. Geophys. Res.* **114,** C02024 (2008).
15. Nikurashin, M. & Ferrari, R. Radiation and dissipation of internal waves generated by geostrophic flows impinging on small-scale topography: Theory. *J. Phys. Oceanogr.* **40,** 1055–1074 (2010).
16. Nikurashin, M. & Ferrari, R. Radiation and dissipation of internal waves generated by geostrophic flows impinging on small-scale topography: Application to the Southern Ocean. *J. Phys. Oceanogr.* **40,** 2025–2042 (2010).
17. Ferrari, R. A frontal challenge for climate models. *Science* **332,** 316–317 (2011).
18. Molemaker, M. J., McWilliams, J. C & Capet, X. Balanced and unbalanced routes to dissipation in an equilibrated Eady flow. *J. Fluid Mech.* **654,** 35–63 (2010).
19. Polzin, K. L., Toole, J. M., Ledwell, J. R. & Schmitt, R. W. Spatial variability of turbulent mixing in the abyssal ocean. *Science* **276,** 93–96 (1997).
20. Ledwell, J. R. *et al.* Evidence for enhanced mixing over rough topography. *Nature* **403,** 179–182 (2000).
21. Heywood, K. J., Naveira Garabato, A. C. & Stevens, D. P. High mixing rates in the abyssal Southern Ocean. *Nature* **415,** 1011–1014 (2002).
22. Winters, K. B., Lombard, P. N., Riley, J. J. & DÁsaro, E. A. Available potential energy and mixing in density-stratified fluids. *J. Fluid Mech.* **289,** 115–128 (1995).
23. Ilicak, M., Adcroft, A. J., Griffies, S. M. & Hallberg, R. W. Spurious dianeutral mixing and the role of momentum closure. *Ocean Model.* **45–46** (2012).
24. Stammer, D. Global characteristics of ocean variability estimated from regional TOPEX/POSEIDON altimeter measurements. *J. Phys. Oceanogr.* **27,** 1743–1769 (1997).
25. Stammer, D. On eddy characteristics, eddy transports, and mean flow properties. *J. Phys. Oceanogr.* **28,** 727–739 (1998).
26. Ozgokmen, T. M., Poje, A. C., Fischer, P. F. & Haza, A. C. Large eddy simulations of mixed layer instabilities and sampling strategies. *Ocean Model.* **39,** 311–331 (2011).
27. Marshall, J., Adcroft, A. J., Hill, C., Perelman, L. & Heisey, C. A finite-volume, incompressible (Navier–Stokes) model for studies of the ocean on parallel computers. *J. Geophys. Res.* **102,** 5753–5766 (1997).

Author contributions

M.N. performed the numerical experiments and led the analysis of the results and writing of the paper. M.N. and G.K.V. were responsible for the overall design of the experiments, interpretation of the results and writing of the paper. A.A. contributed to the design of the experiments and the interpretation of the results.

Additional information

Reprints and permissions information is available online at www.nature.com/reprints. Correspondence and requests for materials should be addressed to M.N.

Competing financial interests

The authors declare no competing financial interests.